Petroleum Science 22 (2025) 1370–1379

Contents lists available at ScienceDirect

Petroleum Science

journal homepage: www.keaipublishing.com/en/journals/petroleum-science

Original Paper

Mesoporogen-free synthesis of hierarchical SAPO-11 from kaolin for hydroisomerization of *n*-alkanes

Chan Wang [a, b], Zhao-Quan Chi [a], Shu Liu [a], Si-Jia Tan [a], Jing-Dong Xu [c], Tie-Sen Li [a, b, *], Ting-Hai Wang [a, b], Yuan-Yuan Yue [a, b, **]

[a] National Engineering Research Center of Chemical Fertilizer Catalyst, College of Chemical Engineering, Fuzhou University, Fuzhou, 350002, Fujian, China
[b] Qingyuan Innovation Laboratory, Quanzhou, 362801, Fujian, China
[c] Sinochem Quanzhou Energy Technology Co., Ltd., Quanzhou, 362000, Fujian, China

ARTICLE INFO

Article history:
Received 19 December 2023
Received in revised form
27 October 2024
Accepted 28 October 2024
Available online 30 October 2024

Edited by Min Li

Keywords:
SAPO-11
Hierarchical pore
Kaolin
Hydroisomerization
High-octane gasoline

ABSTRACT

Hierarchical SAPO-11, featuring both micropore and mesopore channels, demonstrates an outstanding performance in high-octane gasoline production. In this work, we propose an economic and effective approach to directly fabricate hierarchical SAPO-11 molecular sieve from natural kaolin, eliminating the need for mesoporogens. The systematic characterization results show that the kaolin-derived SAPO-11 possesses abundant micro-mesoporous structure and more Brønsted (B) acid sites on the external surface in contrast with the conventional SAPO-11 prepared employing silica sol as silicon source as well as SAPO-11 synthesized with the assist with of poly(ethylene oxide)-block-poly(propylene oxide)-block-poly(ethylene oxide) (F127). The analysis of the formation process reveals that the kaolin not only provides silicon source for the SAPO-11 crystal growth, but also offers confined environment for crystal growth along the preferential orientation, resulting in the generation of the microporous and mesoporous structure. Benefiting from these unique properties, the kaolin-derived Pt/SAPO-11 exhibits considerably improved selectivity for di-branched C_8 isomers in *n*-octane hydroisomerization.

1. Introduction

Amidst the thriving automobile industry, the demand for high-octane gasoline is on the rise (Perera, 2017; Akhmedov and Al-Khowaiter, 2007). A key technology in meeting this demand is the hydroisomerization of low-octane C_5–C_8 *n*-alkanes to their branched isomers (Yu et al., 2020). The development of catalysts that efficiently convert these C_5–C_8 *n*-alkanes into multi-branched alkane isomers is the core of hydroisomerization processes. Bifunctional catalyst based on metal supported aluminosilicates and silicoaluminophosphate (SAPO) molecular sieves are widely applied in the *n*-alkanes hydroisomerization. Among these, SAPO-11 molecular sieve derived bifunctional catalysts have garnered significant attention due to their outstanding hydroisomerization performance (Velazquez et al., 2023; Meriaudeau et al., 1997; Liu et al., 2015; Gao et al., 2020; Wu et al., 2023; Wang et al., 2021). The distinctive pore structure (AEL topological structure) and mild acidity bestow superior hydroisomerization performance on SAPO-11 based catalysts, especially for the production of mono-branched alkane isomers (del Campo et al., 2021).

However, the formation of di-branched alkane are difficult owing to the narrow channel of SAPO-11, which restricting the accessibility of internal active sites and the diffusion of larger products. In the hydroisomerization of *n*-alkanes, it has been established that the pore mouth at the external surface of SAPO-11 grains as an accessible active site where the di-branched alkane isomers are formed (Wang et al., 2021; Chen N. et al., 2022). Therefore, enhancing the external specific surface area (ESSA) of SAPO-11 presents a potential avenue to boost the production of di-branched isomers for the *n*-alkanes hydroisomerization process.

To increase the ESSA of SAPO-11, various organic mesoporogens and crystal growth inhibitors have been introduced into the synthesis system of microporous SAPO-11. These additives aim to create mesopores and decrease crystal size during crystallization. Choi et al. (2006) employed organosilane as a mesoporogen to produce mesoporous SAPO-11. Fan et al. (2012) presented a

* Corresponding author.
** Corresponding author.
E-mail addresses: litiesen@fzu.edu.cn (T.-S. Li), yueyy@fzu.edu.cn (Y.-Y. Yue).

https://doi.org/10.1016/j.petsci.2024.10.009

methodology for creating hierarchical SAPO-11 by introducing tetradecylphosphoric acid into the synthesis system. Zhang et al. (2017) synthesized SAPO-11 nanosheets with the assistance of polyhexamethylene biguanide hydrochloride. Wen et al. (2021) produced various hierarchical SAPO-11 using anionic surfactant sodium dodecylbenzene sulfonate as a dispersant. Dai et al. (2023) synthesized b-axis oriented flower-like SAPO-11 in organosilicon compounds-containing system. Wen et al. (2019) obtained hierarchical SAPO-11 by combining poly(ethylene oxide)-block-poly(propylene oxide)-block-poly(ethylene oxide) (F127) and $ScCO_2$ as mesoporous templates at a low crystallization temperature. Our group reported a hierarchical SAPO-11 with smaller crystal size by utilizing both of cetyltrimethylammonium bromide (CTAB) and F127 (Zhang et al., 2018). Wang et al. (2023) introduced dual additives CTAB and KF to fabricate SAPO-11 with a lamellar structure and flower-like morphology. Therefore, the synthesis of SAPO-11 with a large ESSA traditionally relies on the use of expensive organic mesoporogens/inhibitors. These practices not only greatly increase the synthesis cost but also results in the emission of carbon dioxide and nitrogen oxides during calcination, exacerbating the greenhouse effect.

Utilizing natural aluminosilicate minerals as starting materials has enabled the synthesis of hierarchical molecular sieves without the need for organic mesoporogen. This approach not only eliminates the requirement for expensive and hazardous organic mesoporogen but also establishes an environmentally sustainable fabrication pathway (Maghfirah et al., 2020). It has been confirmed that aluminosilicate minerals provide the Al and Si sources for molecular sieves synthesis. Furthermore, the meso/macropores inherent in aluminosilicate minerals can be preserved in the final molecular sieve product. Various hierarchical molecular sieves with diverse topologies, such as SAPO-34, ZSM-5, Y and Beta have been successfully synthesized from kaolin, rectorite and diatomite without the assist of mesoporogens (Zhu et al., 2009; Yue et al., 2020; Wang et al., 2022; Zheng et al., 2022). Nonetheless, the synthesis of SAPO-11 with a hierarchical pore structure using natural aluminosilicate minerals has not been reported thus far.

In this contribution, we present a mesoporogen-free strategy for synthesizing hierarchical SAPO-11 from kaolin. A comprehensive investigation into the physicochemical properties and hydroisomerization performance of the SAPO-11 was conducted and compared with those of a conventional microporous SAPO-11 and a hierarchical SAPO-11 synthesized using F127 as a mesoporogen. Additionally, we explored the mechanism behind the formation of the hierarchical SAPO-11 molecular sieve from kaolin.

2. Experimental

2.1. Synthesis of SAPO-11 molecular sieves

A hierarchical SAPO-11 (SP-11-K) was directly constructed from natural kaolin clay via a mesoporogen-free strategy. Initially, the kaolin was calcined at 800 °C for 6 h, followed by dissolving the calcined kaolin in H_3PO_4. After being stirred at 80 °C for 2 h, deionized water, pseudoboehmite and DPA were added to the above mixture and stirred for additional 4 h. Subsequently, the resulting gel, with a molar composition of 1.0 Al_2O_3:0.3 SiO_2:0.9 P_2O_5:1.4 DPA:100 H_2O, was sealed in a stainless-steel autoclave and crystallized at 180 °C for 24 h. The SAPO-11 sample was obtained by filtration, drying at 100 °C for 4 h and calcination at 600 °C for 6 h.

For a comprehensive comparison, a conventional SAPO-11 (SP-11-S) was synthesized by using the silica sol and pseudoboehmite as starting materials. Another reference sample (SP-11-SF) was prepared by adding F127 as a mesoporogen into the synthesis system of SP-11-S, with an F127/Al_2O_3 molar ratio of 0.001. SP-11-S and SP-11-SF were synthesized through the same procedure as for preparing SP-11-K.

2.2. Preparation of Pt/SAPO-11 catalysts

The Pt doped SAPO-11 catalysts (Pt/SAPO-11 = 0.5 wt%) were prepared according to the incipient wetness impregnation procedure. Initially, the SAPO-11 sample was impregnated with an aqueous H_2PtCl_6 (Aldrich) solution for 24 h. Subsequently, the impregnated sample was dried at 120 °C for 2 h and then calcined in the air at 450 °C for 2 h. The catalysts derived from SP-11-K, SP-11-S and SP-11-SF were denoted as Pt/SP-11-K, Pt/SP-11-S and Pt/SP-11-SF, respectively.

2.3. Characterizations

The physicochemical properties of all samples were characterized by X-ray diffraction (XRD), scanning electron microscope (SEM), high resolution transmission electron microscopy (HRTEM), N_2 adsorption-desorption, Temperature programmed desorption of ammonia (NH_3-TPD), Pyridine infrared (Py-IR) and 2,6-dimethylpyridine infrared (2,6-DMPy-IR) spectra and ^{29}Si magic-angle-spinning nuclear magnetic resonance (MAS NMR) spectra. The detailed measure conditions are presented in the supporting information (SI).

2.4. Hydroisomerization of n-octane

The catalytic performance of the catalysts was evaluated by using *n*-octane hydroisomerization as a model reaction in a 10 mL continuously flowing fixed-bed microreactor. Following reduction in a hydrogen flowing at 400 °C for 4 h, the catalysts were tested at temperatures ranging from 280 to 360 °C, a pressure of 1.5 MPa, an H_2/*n*-octane volumetric ratio of 300, and a weight hourly space velocity (WHSV) of 1.5 h^{-1}. A Shimadzu GC-2014 gas chromatograph (GC) was utilized to analyze the product composition.

The parameters of *n*-octane conversion (C), branched C_8 isomer selectivity (S_B), di-branched C_8 isomer selectivity (S_{DB}), and cracking selectivity (S_C) were used to evaluate the hydroisomerization performance. These parameters are defined as:

$$C = \frac{n_i - n_u}{n_i} \times 100\% \quad (1)$$

$$S_B = \frac{n_B}{n_i - n_u} \times 100\% \quad (2)$$

$$S_{DB} = \frac{n_{DB}}{n_i - n_u} \times 100\% \quad (3)$$

$$S_C = (100\% - S_B) \times 100\% \quad (4)$$

where n_i and n_u are the moles of *n*-octane in the feedstock and product, respectively; n_B and n_{DB} denote the moles of branched C_8 isomers and di-branched C_8 isomers in the product, respectively. Turn-over frequency (TOF) values of the three catalysts were obtained at 280 °C with conversion below 20%, based on the number of reacted *n*-octane molecules per second and per medium and strong B acid sites (BAS).

3. Results and discussion

3.1. Phase structure

The XRD patterns of SP-11-S, SP-11-SF and SP-11-K are displayed in Fig. 1. All of the samples exhibit characteristic diffraction peaks ascribed to the AEL topology structure (Gao et al., 2022), with no additional peaks observed. This indicates that a pure-phase SAPO-11 molecular sieve has been successfully synthesized from natural kaolin clay.

3.2. Morphology

The SEM images of the three SAPO-11 samples are shown in Fig. 2. SP-11-S and SP-11-SF exhibit pseudo-spherical morphologies with a particle size of 5–8 μm and rough surfaces (Fig. 2(a) and (c)). The high magnification SEM images (Fig. 2(b) and (d)) show that the particles of SP-11-S and SP-11-SF possess a lamellar structure on the surface, with the crystallites on the surface of SP-11-SF appearing smaller and more fragmented than SP-11-S. SP-11-K displays a distinct column morphology with a particle size of 3–5 μm, featuring numerous trapezoidal grains growing in the axial direction on the particle surface (Fig. 2(e) and (f)). The pronounced differences among SP-11-S, SP-11-SF and SP-11-K are evident, with the unique morphology of the SP-11-K likely attributed to kaolin.

3.3. Textural properties

The N_2 adsorption-desorption isotherms and the pore size distributions of SP-11-K, SP-11-SF and SP-11-S are illustrated in Fig. 3. All three samples exhibit type IV isotherms with H3-type hysteresis loop in the relative pressure range of $0.45 < P/P_0 < 1.0$ (Fig. 3(a)), indicative of N_2 capillary condensation in the mesopores. It indicates the existence of a mesoporous structure within the samples. The pore size distributions (Fig. 3(b)), calculated using the BJH model from the adsorption branch, further confirm the presence of mesopores, approximately 15 nm in size, in all three samples). Importantly, the mesopore content follows the sequence: SP-11-S < SP-11-SF < SP-11-K). This suggests that SP-11-K possesses more mesopore structure than SP-11-S, and SP-11-SF, even though the latter was synthesized with mesoporogen F127. Combining these results with the SEM results (Fig. 2), it is reasonable to infer that the mesopores are formed between the stacked nanocrystallites.

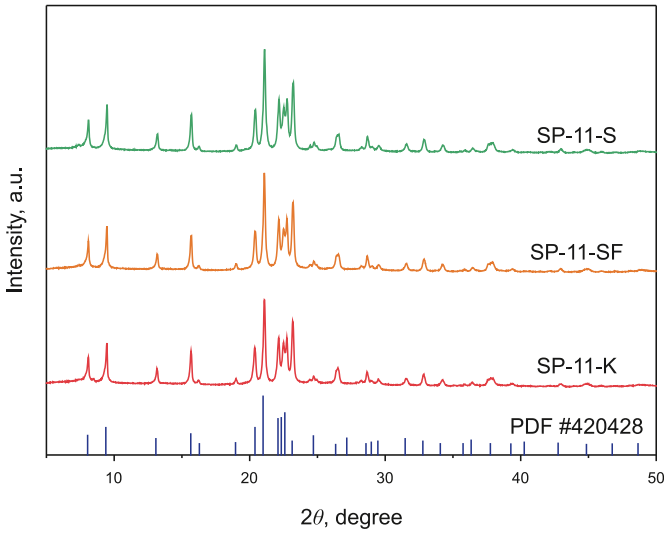

Fig. 1. XRD patterns of SP-11-S, SP-11-SF and SP-11-K.

The texture properties of SP-11-S, SP-11-SF and SP-11-K are summarized in Table 1. In comparison with SP-11-S, the ESSA and mesopore volume of SP-11-SF increase (85 vs 64 m^2/g, 0.14 vs 0.11 cm^3/g), whereas the micropore specific surface area and micropore volume decrease (135 vs 156 m^2/g, 0.07 vs 0.09 cm^3/g), which is similar to other hierarchical zeolites synthesized with organic mesoporogen (Egeblad et al., 2008). For SP-11-K, the ESSA and mesopore volume are significantly higher than those of SP-11-S (103 vs 64 m^2/g, 0.19 vs 0.11 cm^3/g), even higher than those of SP-11-SF (103 vs 85 m^2/g, 0.19 vs 0.14 cm^3/g), while the micropore specific surface area and micropore volume are well maintained. These results indicate that both mesoporous and microporous structure of the kaolin-derived SAPO-11 are promoted.

3.4. Acidity properties

NH_3-TPD experiments were carried out to evaluate the acidic properties of the SAPO-11 samples, and the NH_3-TPD curves are shown in Fig. 4. The peaks located at 150–185 °C correspond to the NH_3 desorption from weak acid sites (AS), while peaks located at 310–340 °C are associated with NH_3 desorption from medium and strong AS (Z.P Chen et al., 2022). In the case of SP-11-K, NH_3 desorption temperatures were measured at 215 and 340 °C, exceeding those of SP-11-S and SP-11-SF (195 and 320 °C), suggesting the stronger acid strength of SP-11-K. The quantity of AS was determined through the NH_3-TPD profiles and is listed in Table 2. The amount of AS on SP-11-K and SP-11-S is nearly equal, suggesting that the silicon from kaolin is integrated into the framework of SP-11-K, functioning as acid sites similarly to silica sol. Contrastingly, for SP-11-SF, the amount of total AS, particularly medium and strong AS, is considerably lower than those of SP-11-K and SP-11-S, suggesting the introduction of F127 notably reduces the acidity of SAPO-11.

To identify the AS types present in the three SAPO-11 samples, Py-IR characterization was performed, and the spectra are given in Fig. 5. The bands at 1540 and 1455 cm^{-1} are attributed to the Py molecules adsorbed on the B and Lewis (L) AS, respectively (Ma et al., 2023). The Py-IR spectra were recorded at 200 and 350 °C to calculate the amount of total and medium/strong AS, respectively, with the results outlined in Table 2. The amount of total and medium/strong B and L AS over SP-11-K (118.6 and 60.4 μmol/g) closely approximate those of SP-11-S (116.5 and 58.7 μmol/g). Unlike SP-11-S, SP-11-K possesses less total B (85.6 vs 95.2 μmol/g) and medium/strong B (44.2 vs 49.4 μmol/g) AS, but more total L (30.9 vs 23.4 μmol/g) and medium/strong L (14.5 vs 11.0 μmol/g) AS. As for SP-11-SF, the amount of total as well as medium/strong B and L AS are much lower than those of SP-11-S and SP-11-K, which is in accord with the NH_3-TPD result.

2,6-DMPy-IR characterization was further carried out to explore the distribution of BAS, as shown in Fig. 6. The dynamic diameter of 2,6-DMPy molecule (0.67 nm) is larger than the pore diameter of SAPO-11 molecular sieve (0.39 nm × 0.64 nm), thus 2,6-DMPy can only be absorbed at the external surface of SAPO-11 molecular sieve (Ibrahim et al., 2021). In Fig. 6, the signal around 1640 cm^{-1} is attributed to the adsorption of 2,6-DMPy on the BAS at the external surface of the SAPO-11 samples (Wen et al., 2021). The amount of total and medium/strong BAS at the SAPO-11 external surface were determined by 2,6-DMPy-IR at 200 and 350 °C, respectively, with the results presented in Table 2. Although the BAS over SP-11-K is less than that of SP-11-S as confirmed by Py-IR, the amount of total

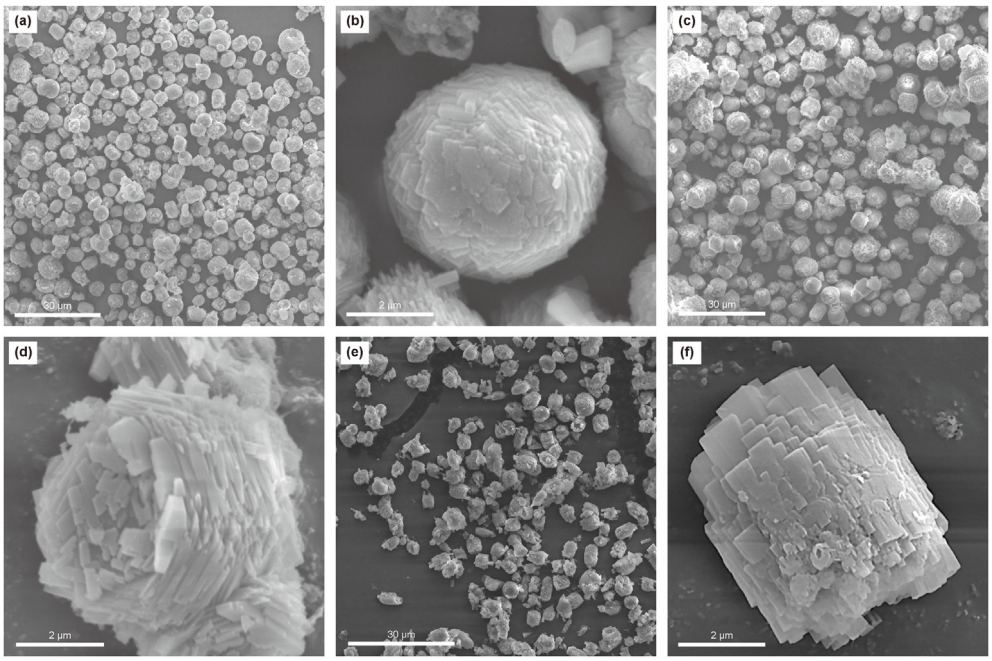

Fig. 2. SEM images of SP-11-S (**(a), (b)**), SP-11-SF (**(c), (d)**) and SP-11-K (**(e), (f)**).

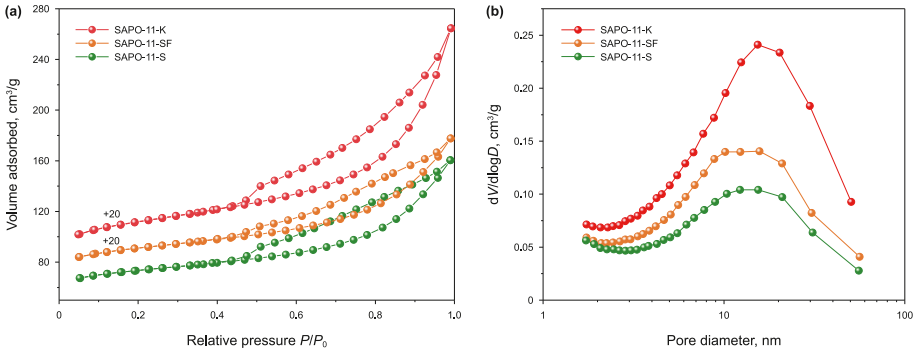

Fig. 3. Nitrogen adsorption-desorption isotherms **(a)** and BJH pore size distributions curves **(b)** of SP-11-K, SP-11-SF and SP-11-S.

Table 1
Textural properties of SP-11-S, SP-11-SF and SP-11-K.

Sample	S_{BET}, m^2/g	S_{micro}, m^2/g	S_{ext}, m^2/g	V_{total}, cm^3/g	V_{micro}, cm^3/g	V_{meso}, cm^3/g
SP-11-S	220	156	64	0.20	0.09	0.11
SP-11-SF	220	135	85	0.21	0.07	0.14
SP-11-K	251	148	103	0.27	0.08	0.19

and medium/strong BAS at the external surface of SP-11-K (9.6 and 7.5 μmol/g) are significantly higher than those of SP-11-S (8.2 and 6.3 μmol/g), respectively. Combining the acidity results as well as the above SEM and N_2 adsorption-desorption results, it can be inferred that the SP-11-K, with a larger external specific surface area, can generate more BAS at the pore mouths. By contrast, despite of large ESSA, the BAS at the external surface of SP-11-SF is notably less than that of SP-11-S, possibly due to the negative impact of F127 on BAS exposure. Therefore, it can be concluded that SP-11-K synthesized from kaolin possesses both abundant micro-mesoporous structure and enhanced BAS at the external surface, indicating SP-11-K may be the best for the formation of di-branched alkane isomers.

3.5. Chemical environments

The acidity of SAPO-11 molecular sieves is well-established to arise from silicon atoms integrated into the $AlPO_4$-11 framework, making the acidity properties contingent on the manners of silicon substitution. To elucidate the chemical environment of silicon in the three SAPO-11 samples, ^{29}Si MAS NMR experiments were carried out, and the spectra are presented in Fig. 7. The signal at −91 ppm is assigned to the Si(4Al) species within the SAPO domain, while signals at −85, −97, −102, −108 and −113 ppm represent the Si(4Al), Si(3Al), Si(2Al), Si(1Al) and Si(4Si) species in the silica-alumina (SA) domain, respectively (Yu et al., 2020). The spectra were deconvolved into six distinct peaks using Gaussian

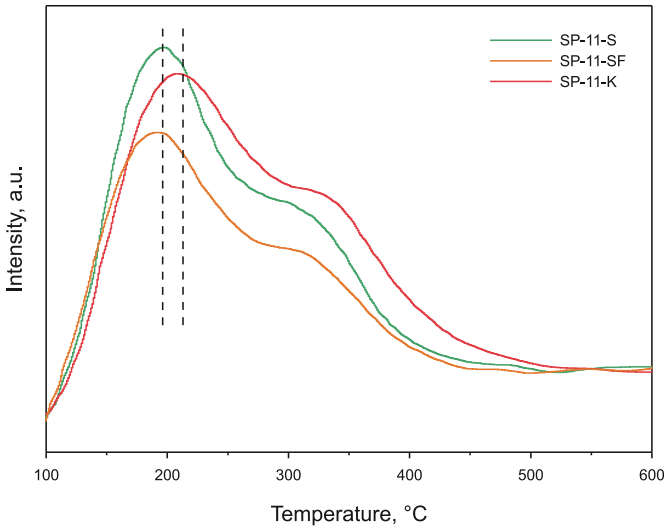

Fig. 4. NH_3-TPD curves of SP-11-S, SP-11-SF and SP-11-K.

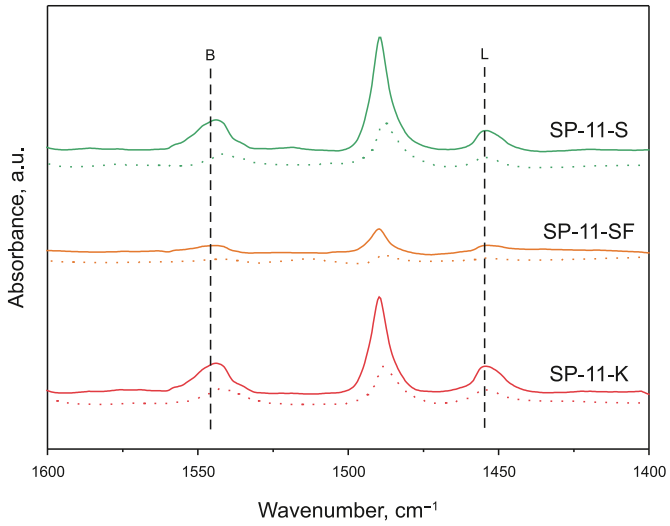

Fig. 5. Py-IR spectra of SP-11-S, SP-11-SF and SP-11-K at 200 °C (solid) and 350 °C (dashed).

fitting, and the proportion of different Si species in the three SAPO-11 samples is shown in Table S3. The Si(nAl) ($4 < n < 0$) proportion in the three samples decreases in the sequence of SP-11-S (57.8%) > SP-11-K (57.0%) > SP-11-SF (50.1%), mirroring the trend observed in the amount of medium/strong BAS in Table 2 (SP-11-S: 49.4 μmol/g > SP-11-K: 44.2 μmol/g > SP-11-SF: 26.3 μmol/g). Typically, the Si (nAl) ($4 < n < 0$) species associated with the medium/strong BAS that facilitate the isomerization of alkanes (Lyu et al., 2018; Lu et al., 2021). Moreover, the Si(4Si) species in SP-11-SF are notably higher than SP-11-S and SP-11-K, which contributes to a significant reduction in the amount of AS over SP-11-SF, as confirmed by NH_3-TPD and Py-IR results.

3.6. Formation mechanism of the hierarchical SAPO-11 from kaolin

To understand the formation of hierarchical SAPO-11 molecular sieves, the whole formation process of SAPO-11 from kaolin was studied.

Prior to the synthesis of the hierarchical SAPO-11, raw kaolin was pretreated by calcination at 800 °C for 6 h to activate the Al and Si species. This step was necessary due to the low reactivity of raw kaolin with the mixture of DPA, H_3PO_4, Al_2O_3 and H_2O. The XRD patterns of both the raw kaolin and calcined kaolin (kaolin-C) are shown in Fig. 8. The peaks at 2θ of 12.4° and 24.9° of raw kaolin are characteristic of the kaolinite phase (Lima et al., 2019). After calcination, the unique XRD peaks of kaolinite phase disappears and are replaced by broad background corresponding to the amorphous phase, indicating the transition from crystalline kaolinite to disordered metakaolin. It is known that during the calcination water molecules are removed from the alumina

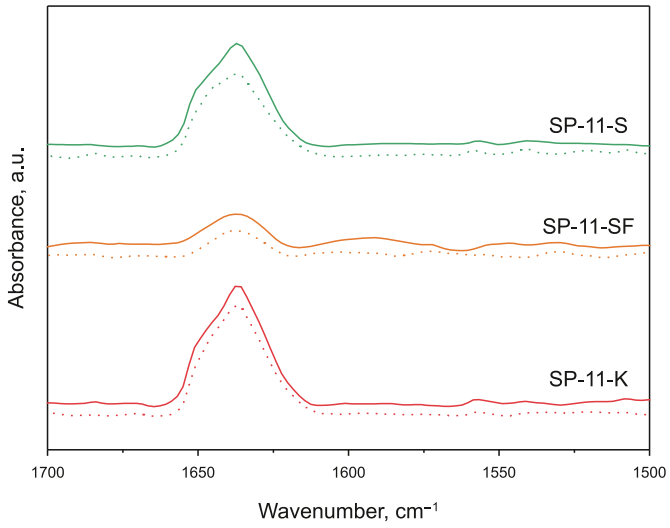

Fig. 6. 2,6-DMPy-IR spectra of SP-11-S, SP-11-SF and SP-11-K at 200 °C (solid) and 350 °C (dashed).

octahedral layer during calcination, facilitating the transformation of octahedral coordinated Al into tetra- and penta-coordinated Al units, and thus these Al units become the activated aluminium source for synthesizing the molecular sieve. In contrast, the silicon-oxygen tetrahedral layers remain almost intact (Zhu et al., 2009). When kaolin-C was employed for SAPO-11 synthesis using the

Table 2
Acidity properties of the SAPO-11 samples determined by NH_3-TPD, Py-IR and 2,6-DMPy-IR.

Sample	NH_3-TPD, mmol/g		Py-IR, μmol/g				2,6-DMPy-IR, μmol/g	
	Weak acid sites	Medium/strong acid sites	Total acid sites		Medium/strong acid sites		Total acid sites on the external surface	Medium/strong acid sites on the external surface
			B	L	B	L	B	B
SP-11-S	0.27	0.23	95.2	23.4	49.4	11.0	8.2	6.3
SP-11-SF	0.21	0.11	50.2	13.6	26.3	5.6	4.7	2.2
SP-11-K	0.25	0.23	85.6	30.9	44.2	14.5	9.6	7.5

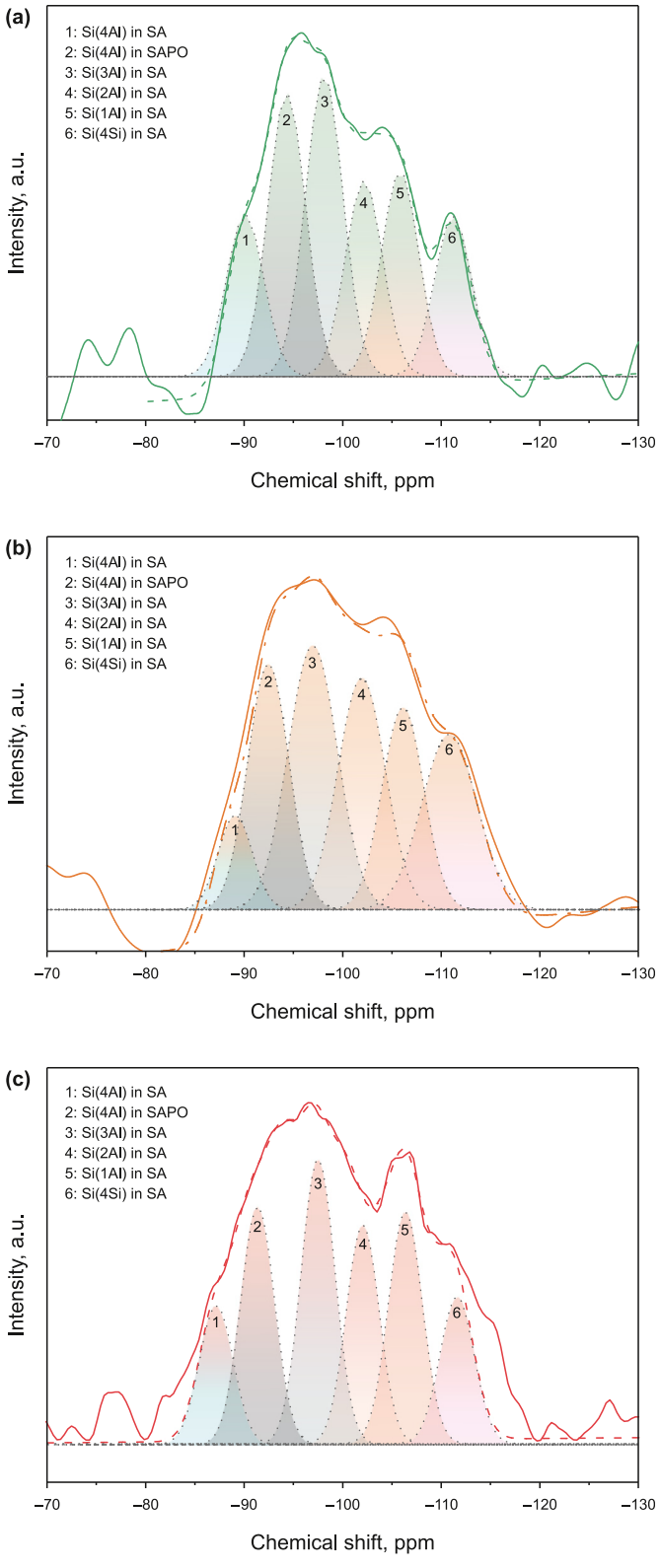

Fig. 7. ^{29}Si MAS NMR spectra of SP-11-S (**a**), SP-11-SF (**b**) and SP-11-K (**c**).

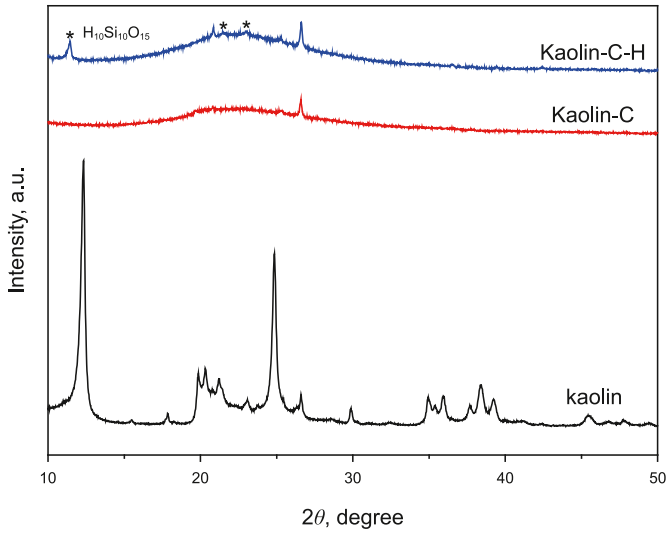

Fig. 8. XRD patterns of raw kaolin, calcined kaolin (kaolin-C) and H_3PO_4-treated kaolin-C (kaolin-C-H).

conventional procedure, some unreacted metakaolin was observed in the synthesized SAPO-11 product. It is inferred that the silica layers of metakaolin may strongly inhibit the transformation of kaolin into SAPO-11.

To activate the silica layers, the kaolin-C was further treated with H_3PO_4 at 80 °C for 2 h. Some characteristic diffraction peaks ascribed to $H_{10}Si_{10}O_{15}$ appeared in the XRD pattern of the H_3PO_4-treated kaolin-C (kaolin-C-H in Fig. 8), indicating the silicon units in kaolin-C are susceptible to H_3PO_4 leaching, thereby leading to the dissolution of silicon units. From the SEM images (Fig. S1), it can be observed that compared to Kaolin and Kaolin-C, the surface of Kaolin-C-H is rougher, indicating that the surface has undergone a certain degree of damage. The surface area of kaolin-C-H (Table S1) further indicate the formation of mesopores by the dissolution of metakaolin in H_3PO_4. The energy-dispersive X-ray (EDX) analysis (Fig. S2) and X-ray fluorescence (XRF) results (Table S2) indicate a drastic reduction in the aluminum content of kaolin-C-H in comparison with kaolin-C. This suggests that both Si and Al units can be dissolved by H_3PO_4, with aluminum units from metakaolin being more readily dissolved than silicon units. When the mixture of kaolin-C and H_3PO_4 was used to synthesize SAPO-11, no residual metakaolin was detected in the product, resulting in the production of pure-phase SAPO-11. The results suggest that the silicon and aluminium units were leached from kaolin-C by the H_3PO_4 treatment, serving as activated silicon and aluminum sources in the synthesis of SAPO-11. Therefore, the H_3PO_4 treatment is a crucial step in the fabrication of SAPO-11 from kaolin.

To reveal the crystallization process of the hierarchical SAPO-11 from kaolin, a series of products were obtained by controlling the crystallization time, and characterized by XRD (Fig. S3), SEM (Fig. 9) and EDX (Figs. 10 and S4). In the initial crystallization stage (0–3 h), XRD patterns of the solid products show no indication of crystalline material, indicating that the growth of SAPO-11 did not start in 0–3 h. Unreacted metakaolin and some irregular particles are observed in the SEM images, and the EDX analysis shows that the unreacted metakaolin contains mainly Si (70%–90%). After crystallization for 6 h, the characteristic peaks of SAPO-11 appear in the XRD pattern of the product, the corresponding column morphological SAPO-11 crystals can be found in the SEM image, while the Si content in amorphous metakaolin drops sharply at the same time. It is probably because that the Si transfers from the metakaolin into SAPO-11 crystals. As the crystallization time is prolonged to 9–12 h, the XRD signal of SAPO-11 becomes more intensive, and the Si content in the SAPO-11 crystals increases (Fig. 10). After 24 h of crystallization, crystal growth is almost complete, with the Si content in the SAPO-11 crystals reaching its maximum. Notably,

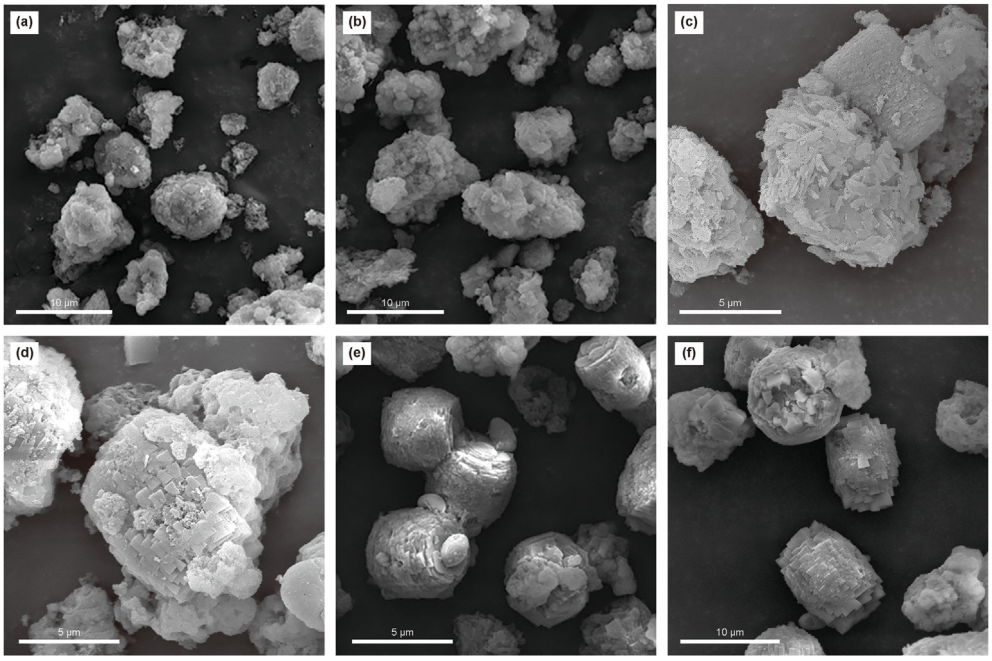

Fig. 9. SEM images of the products obtained after crystallization for **(a)** 0 h, **(b)** 3 h, **(c)** 6 h, **(d)** 9 h, **(e)** 12 h and **(f)** 24 h.

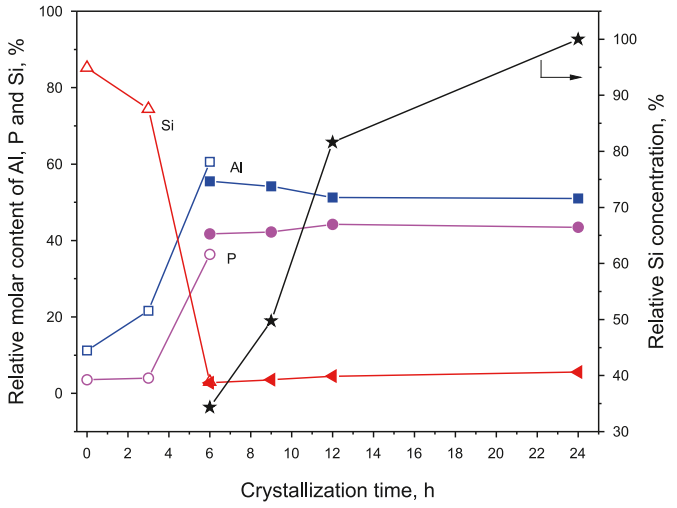

Fig. 10. The relative molar content of Al (square), P (round) and Si (triangle) for amorphous substance (hollow) and SAPO-11 crystal (solid) in the products obtained after crystallization for different time; the concentration of Si relative to its maximum in SAPO-11 crystal obtained after crystallization for different time (pentagram).

during the crystallization process, the surface of the SAPO-11 crystal appears quite rough, and a large number of trapezoidal crystallites grow in the axial direction on the surface of the cylindrical crystal. Zhu et al. (2009) pointed out that the layered structure of kaolin could provide nanoscale confined environment for hierarchical molecular sieve growth. Therefore, our observations draw forth the inference that kaolin provides silicon source for the SAPO-11 crystal growth, and the confined environment between the silica layers simultaneously favors crystal growth along the preferential orientation due to the lower reactivity of silica layers. As a result, a hierarchical SAPO-11 with a distinctive morphology is derived from kaolin.

Based on the above discussion, a schematic illustration for the formation of the hierarchical SAPO-11 from kaolin is proposed, as shown in Fig. 11. The complete transformation process from kaolin to the hierarchical SAPO-11 can be described as follows:

(1) When calcined at 800 °C, the kaolin undergoes dihydroxylation and structural change, transforming into metakaolin. The octahedral Al transforms into tetra- and penta-coordinate Al units, while the silicon-oxygen tetrahedral layers almost maintain intact as in kaolin.
(2) The calcined kaolin is further mixed with H_3PO_4 at 80 °C to activate the silica layers. Following H_3PO_4 treatment, most of the Al and partial Si units in calcined kaolin dissolve, serving as sources of Al and Si for SAPO-11 synthesis, while partial silica layers still remain.
(3) With the interaction with other reactants (DPA and Al_2O_3) and prolonged time of hydrothermal crystallization, the Si units gradually dissolve and participate in the construction of the SAPO-11 framework. Simultaneously, the undissolved silica layers provide a confined environment that facilitates crystal growth along a preferential orientation.
(4) Finally, the crystallites self-assemble into polycrystalline particles, yieldinghierarchical SAPO-11 particles in the form of bunches of trapezoidal crystallites growing in the same direction.

3.7. Catalytic performance in n-octane hydroisomerization

The three obtained Pt/SAPO-11 catalysts were applied to *n*-octane hydroisomerization reaction. TEM images revealed well-defined Pt clusters uniformly dispersed on the external surface of the SAPO-11 crystals, with an average size of approximately 5 nm (Fig. S5). All three catalysts show a similar distribution of Pt, which means their different catalytic performances originate from the physicochemical properties of SAPO-11. The catalytic performances of Pt/SP-11-S, Pt/SP-11-SF and Pt/SP-11-K in *n*-octane hydroisomerization reaction are shown in Fig. 12. At each investigated temperature, Pt/SP-11-K exhibits comparable *n*-octane conversion

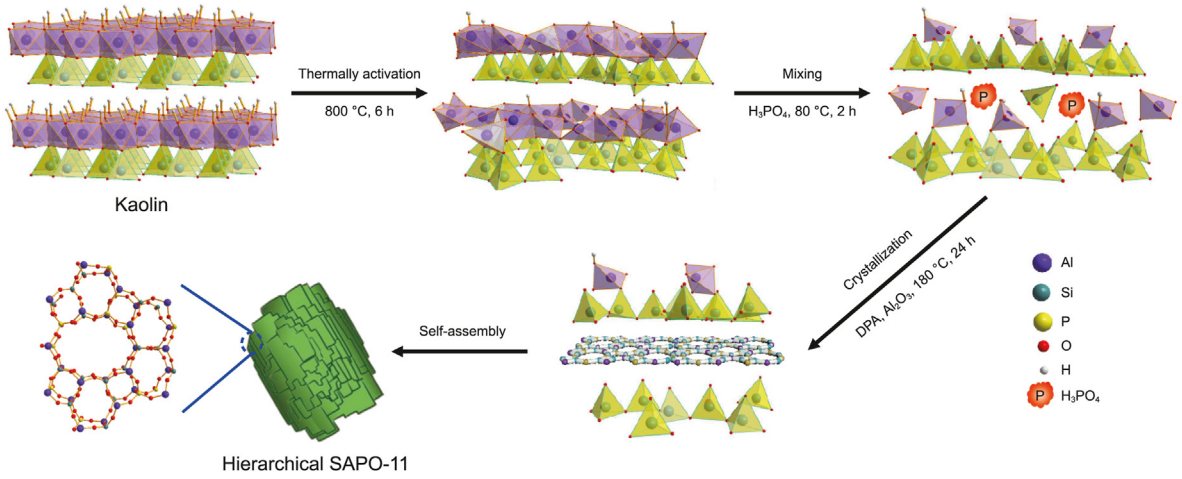

Fig. 11. Schematic illustration of the formation mechanism of the hierarchical SAPO-11 from kaolin.

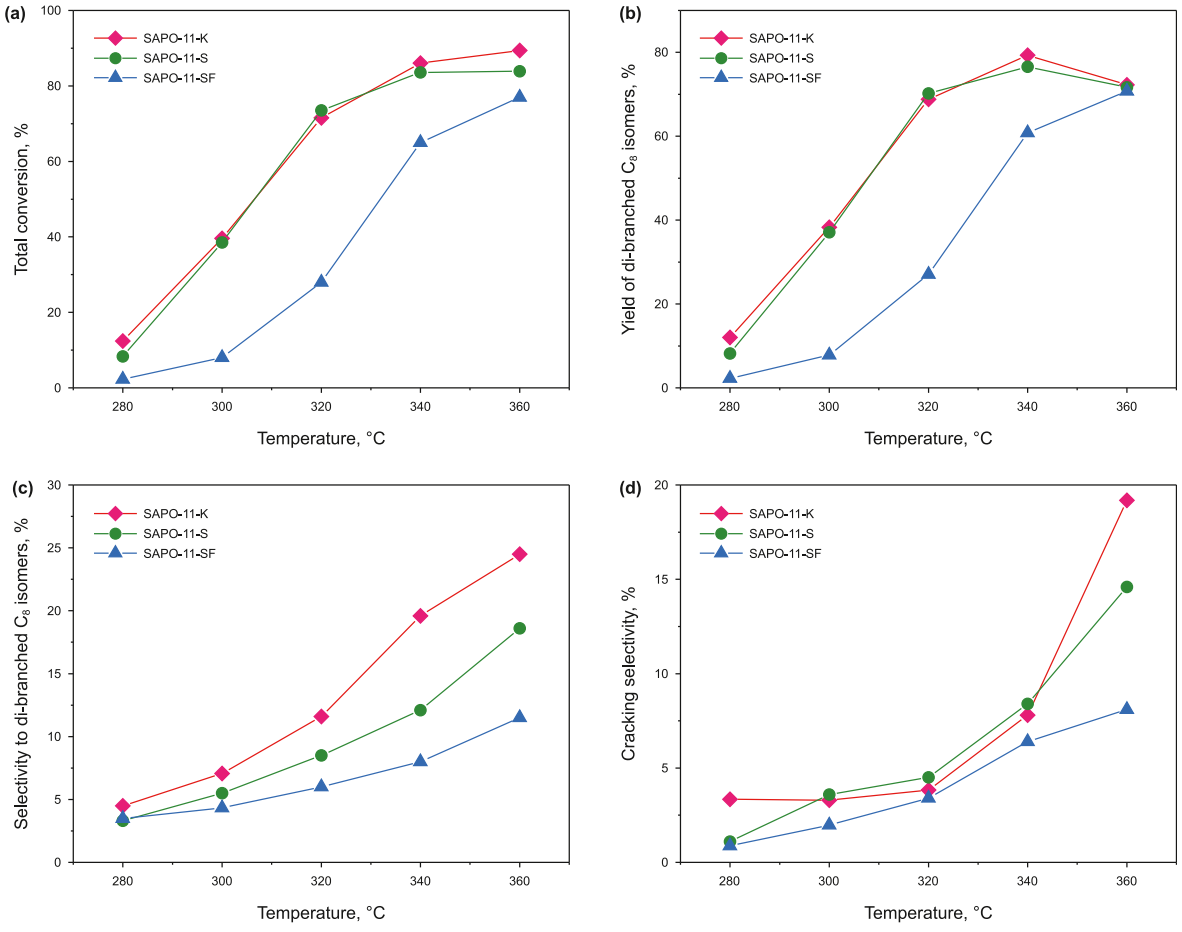

Fig. 12. The *n*-octane conversion **(a)**, di-branched C_8 isomers yield **(b)** and selectivity **(c)**, and cracking selectivity **(d)** over Pt/SP-11-S, Pt/SP-11-SF and Pt/SP-11-K.

(Fig. 12(a)), di-branched C_8 isomers yield (Fig. 12(b)) and cracking selectivity (Fig. 12(d)) to Pt/SP-11-S, but exhibited significantly higher selectivity towards di-branched C_8 isomers (Fig. 12(c)). In the *n*-octane isomerization reaction, the presence of medium and strong B and L AS on SAPO-11 facilitates both *n*-octane isomerization and alkane cracking, while the formation of di-branched isomers is restricted to the BAS near the pore mouths of SAPO-11 crystals (Wu et al., 2023; Wang et al., 2021). Considering the similar medium/strong B and L AS in SP-11-K and SP-11-S (Table 2), their comparable *n*-octane conversion and cracking selectivity were anticipated. SP-11-K with more moderate/strong BAS on the external surface, boosts the selectivity of di-branched isomers. In contrast, Pt/SP-11-SF shows lower conversion, di-branched C_8 isomers selectivity and cracking selectivity due to the lower amount of

AS. Consequently, the excellent *n*-octane conversion and di-branched C_8 isomers selectivity over Pt/SP-11-K can be well interpreted by the synergistic effects of abundant AS and the micro-mesoporous structure of SP-11-K.

At 340 °C, the product distributions (Table S4) indicate that Pt/SP-11-K displays lower selectivity to mono-branched isomers (S_{MB}) but higher selectivity to di-branched C_8 isomers (S_{DB}) compared to Pt/SP-11-S and Pt/SP-11-SF. This alteration is likely due to the promotion of mono-to di-branched isomerization facilitated by the BAS on the external surface of SP-11-K. Furthermore, cracking selectivity is slightly lower in Pt/SP-11-K than in Pt/SP-11-S, attributed to improved mass transport within the micro-mesoporous structure. The superior turnover frequency (TOF) value over Pt/SP-11-K (10.25×10^{-3} s^{-1}) compared to Pt/SP-11-S (6.13×10^{-3} s^{-1}) and Pt/SP-11-SF (3.19×10^{-3} s^{-1}) further underscores the enhanced catalytic properties of SP-11-K.

4. Conclusions

A hierarchical SAPO-11 molecular sieve has been successfully synthesized using a mesoporogen-free strategy facilitated by kaolin. The layered kaolin acts as silicon source and simultaneously provides a confined environment for crystal growth during the formation of SAPO-11. The resulting hierarchical SAPO-11 possesses abundant micro-mesoporous structure and BAS on the external surface, leading to enhanced di-branched isomers selectivity in *n*-octane hydroisomerization. This study provides a facile and cost-effective route for the fabrication of hierarchical SAPO-11 without the assistance of mesoporogen. It suggests the potential for the direct preparation of highly effective hierarchical SAPO molecular sieves from natural aluminosilicate minerals.

CRediT authorship contribution statement

Chan Wang: Writing – review & editing, Writing – original draft, Funding acquisition, Data curation. **Zhao-Quan Chi:** Methodology, Data curation. **Shu Liu:** Data curation. **Si-Jia Tan:** Data curation. **Jing-Dong Xu:** Funding acquisition. **Tie-Sen Li:** Supervision, Conceptualization. **Ting-Hai Wang:** Conceptualization. **Yuan-Yuan Yue:** Supervision, Funding acquisition.

Declaration of competing interest

The authors declare that they have no known competing financial interests or personal relationships that could have appeared to influence the work reported in this paper.

Acknowledgements

The authors greatly thank the National Natural Science Foundation of China (grant 22208054, 22178059 and U23A20113), Natural Science Foundation of Fujian Province, China (grant 2022J01572), Sinochem Quanzhou Energy Technology Co., Ltd. (grant ZHQZKJ-19-F-ZS-0076), and Qingyuan Innovation Laboratory (grant 00121002 and 00523005) for their financial supports.

Appendix A. Supplementary data

Supplementary data to this article can be found online at https://doi.org/10.1016/j.petsci.2024.10.009.

References

Akhmedov, V.M., Al-Khowaiter, S.H., 2007. Recent advances and future aspects in the selective isomerization of high *n*-alkanes. Catal. Rev. 49, 33–139. https://doi.org/10.1080/01614940601128427.

Chen, N., Zhang, J., Gu, Y., et al., 2022. Designed synthesis of MOR zeolites using gemini-type bis(methylpyrrolidinium) dications as structure directing agents and their DME carbonylation performance. J. Mater. Chem. A. 10, 8334–8343. https://doi.org/10.1039/D2TA00451H.

Chen, Z.P., Shi, F.X., Zhou, W.W., et al., 2022. Study on SAPO-11 molecular sieve catalyst with small particle size and hierarchical pores for isomerization of hydrocarbons. Chem. Ind. Eng. Prog. 41, 4767–4781. https://doi.org/10.16085/j.issn.1000-6613.2021-2414 (in Chinese).

Choi, M., Srivastava, R., Ryoo, R., 2006. Organosilane surfactant-directed synthesis of mesoporous aluminophosphates constructed with crystalline microporous frameworks. Chem. Commun. 4380–4382. https://doi.org/10.1039/B612265E.

Dai, X., Cheng, Y., Liu, T., et al., 2023. Novel construction and synthesis mechanism of b-axis oriented flower-like SAPO-11 molecular sieve in OSC-containing system for efficient hydroisomerization of long-chain *n*-alkanes. Chem. Eng. J. 475, 146412. https://doi.org/10.1016/j.cej.2023.146412.

del Campo, P., Martinez, C., Corma, A., 2021. Activation and conversion of alkanes in the confined space of zeolite-type materials. Chem. Soc. Rev. 50, 8511–8595. https://doi.org/10.1039/D0CS01459A.

Egeblad, K., Christensen, C.H., Kustova, M., et al., 2008. Templating mesoporous zeolites. Chem. Mater. 20, 946–960. https://doi.org/10.1021/cm702224p.

Fan, Y., Xiao, H., Shi, G., et al., 2012. Alkylphosphonic acid- and small amine-templated synthesis of hierarchical silicoaluminophosphate molecular sieves with high isomerization selectivity to di-branched paraffins. J. Catal. 285, 251–259. https://doi.org/10.1016/j.jcat.2011.09.037.

Gao, S.B., Zhao, Z., Lu, X.F., et al., 2020. Hydrocracking diversity in *n*-dodecane isomerization on Pt/ZSM-22 and Pt/ZSM-23 catalysts and their catalytic performance for hydrodewaxing of lube base oil. Petrol. Sci. 17, 1752–1763. https://doi.org/10.1007/s12182-020-00500-7.

Gao, M., Zhao, X.H., Xiang, Y.S., et al., 2022. Impact of water amount and seed crystal on SAPO-11 molecular sieve synthesis and isomerization performance. Pet. Process. Petroche. 53, 22–30. http://www.sylzyhg.com/EN/Y2022/V53/I3/22.

Ibrahim, M., Jalil, A.A., Zakaria, W.F.W., et al., 2021. *n*-Hexane hydroisomerization over Zr-modified bicontinuous lamellar silica mordenite supported Pt as highly selective catalyst: molecular hydrogen generated protonic acid sites and optimization. Int. J. Hydrogen Energy 46, 4019–4035. https://doi.org/10.1016/j.ijhydene.2020.11.006.

Lima, E.T.L., Queiroz, L.S., Pires, L.H.D., et al., 2019. Valorization of mining waste in the synthesis of organofunctionalized aluminosilicates for the esterification of waste from palm oil deodorization. ACS Sustain. Chem. Eng. 7, 7543–7551. https://doi.org/10.1021/acssuschemeng.8b05484.

Liu, P., Wu, M.Y., Wang, J., et al., 2015. Hydroisomerization of *n*-heptane over MoP/Hβ catalyst doped with metal additive. Fuel Process. Technol. 131, 311–316. https://doi.org/10.1016/j.fuproc.2014.11.034.

Lu, Y., Yu, Z., Zhan, W., et al., 2021. Regulation of silicon content and coordination environments over Ni/SAPO-11 catalyst synthesized via in-situ dry gel conversion method. Acta Petrol. Sin.: Pet. Process. Sect. 37, 1366–1377. https://doi.org/10.3969/j.issn.1001-8719.2021.06.017 (in Chinese).

Lyu, Y., Liu, Y., He, X., et al., 2018. The regulation of Si distribution and surface acidity of SAPO-11 molecular sieve. Appl. Surf. Sci. 453, 350–357. https://doi.org/10.1016/j.apsusc.2018.05.106.

Ma, Z., Wang, X., Ma, X., et al., 2023. Catalytic roles of acid property in different morphologies of H-ZSM-5 zeolites for syngas-to-aromatics conversion over $ZnCrO_x$/H-ZSM-5 catalysts. Microporous Mesoporous Mater. 349, 112420. https://doi.org/10.1016/j.micromeso.2022.112420.

Maghfirah, A., Ilmi, M.M., Fajar, A.T.N., et al., 2020. A review on the green synthesis of hierarchically porous zeolite. Mater. Today Chem. 17, 100348. https://doi.org/10.1016/j.mtchem.2020.100348.

Meriaudeau, P., Tuan, V.A., Nghiem, V.T., et al., 1997. SAPO-11, SAPO-31, and SAPO-41 molecular sieves: synthesis, characterization, and catalytic properties in *n*-octane hydroisomerization. J. Catal. 169, 55–66. https://doi.org/10.1006/jcat.1997.1647.

Perera, F.P., 2017. Multiple threats to child health from fossil fuel combustion: impacts of air pollution and climate change. Environ. Health Perspect. 125, 141–148. https://doi.org/10.1289/EHP299.

Velazquez, H.D., Ceron-Camacho, R., Mosqueira-Mondragon, M.L., et al., 2023. Recent progress on catalyst technologies for high quality gasoline production. Catal. Rev. 65, 1079–1299. https://doi.org/10.1080/01614940.2021.2003084.

Wang, M., Han, Y., Liu, S., et al., 2021. Pore-mouth catalysis boosting the formation of iso-paraffins from syngas over bifunctional catalysts. Chin. J. Catal. 42, 2197–2205. https://doi.org/10.1016/S1872-2067(20)63770-6.

Wang, Y., Wang, C., Wang, L., et al., 2021. Zeolite fixed metal nanoparticles: new perspective in catalysis. Acc. Chem. Res. 54, 2579–2590. https://doi.org/10.1021/acs.accounts.1c00074.

Wang, C., Xiao, G., Guo, X., et al., 2022. Green synthesis and application of Beta zeolite prepared via mesoscale depolymerization-reorganization strategy. CIE J. 73, 2690–2697 (in Chinese). doi:11949/0438-1157.20220150.

Wang, X., Zhou, Y., Yu, Z., et al., 2023. Synthesis of lamellar structural flower-like SAPO-11 molecular sieves with hierarchical pores for enhanced selectivity of isomeric alkanes in hydroisomerization. Ind. Eng. Chem. Res. 62, 6394–6415. https://doi.org/10.1021/acs.iecr.2c04587.

Wen, C., Wang, X., Xu, J., et al., 2019. Hierarchical SAPO-11 molecular sieve-based catalysts for enhancing the double-branched hydroisomerization of alkanes. Fuel 255. https://doi.org/10.1016/j.fuel.2019.115821.

Wen, C.L., Xu, J.D., Wang, X.M., et al., 2021. *n*-Nonane hydroisomerization over

hierarchical SAPO-11-based catalysts with sodium dodecylbenzene sulfonate as a dispersant. Petrol. Sci. 18, 654–666. https://doi.org/10.1007/s12182-021-00544-3.

Wu, Q., Yuan, J., Guo, C., et al., 2023. The hydroisomerization of *n*-hexadecane over Pd/SAPOs bifunctional catalysts with different opening size: features of the diffusion properties in pore channels and the metal-acid synergistic catalysis. Fuel Process. Technol. 244, 107692. https://doi.org/10.1016/j.fuproc.2023.107692.

Yu, G., Chen, X., Xue, W., et al., 2020. Melting-assisted solvent-free synthesis of SAPO-11 for improving the hydroisomerization performance of n-dodecane. Chin. J. Catal. 41, 622–630. https://doi.org/10.1016/S1872-2067(19)63466-2.

Yue, Y., Zhu, H., Wang, T., et al., 2020. Green fabrication of hierarchical zeolites from natural minerals. Natl. Sci. Rev. 7, 1632–1634. https://doi.org/10.1093/nsr/nwaa197.

Zhang, F., Liu, Y., Sun, Q., et al., 2017. Design and preparation of efficient hydroisomerization catalysts by the formation of stable SAPO-11 molecular sieve nanosheets with 10-20 nm thickness and partially blocked acidic sites. Chem. Commun. 53, 4942–4945. https://doi.org/10.1039/C7CC01519D.

Zhang, P., Liu, H., Yue, Y., et al., 2018. Direct synthesis of hierarchical SAPO-11 molecular sieve with enhanced hydroisomerization performance. Fuel Process. Technol. 179, 72–85. https://doi.org/10.1016/j.fuproc.2018.06.012.

Zheng, T., Liu, H., Zhang, R., et al., 2022. Research progress on mesoscale activation of natural aluminosilicate minerals based on green synthesis of molecular sieve. CIE J. 73, 2334–2351. https://doi.org/10.11949/0438-1157.20220160.

Zhu, J., Cui, Y., Wang, Y., et al., 2009. Direct synthesis of hierarchical zeolite from a natural layered material. Chem. Commun. 3282–3284. https://doi.org/10.1039/B902661D.